*Anal. Chem.* **2002,** *74,* 5350−5357

# Detection of Flowing Fluorescent Particles in a Microcapillary Using Fluorescence Correlation Spectroscopy

Beno H. Kunst,[†] Arjen Schots,[‡] and Antonie J. W. G. Visser*[,†,§]

*MicroSpectroscopy Centre, Laboratory of Biochemistry, Wageningen University, Dreijenlaan 3, 6703 HA, Wageningen, The Netherlands, Laboratory of Molecular Recognition and Antibody Technology, Wageningen University, Binnenhaven 10, 6709 PD Wageningen, The Netherlands, and Department of Structural Biology, Faculty of Earth and Life Sciences, Vrije Universiteit, De Boelelaan 1087, 1081 HV Amsterdam, The Netherlands*

**Capillary flow experiments are described with fluorescent molecules, bacteria, and microspheres using fluorescence correlation spectroscopy as an analytical tool. The flow velocity in the microcapillary is determined by fitting autocorrelation traces with a model containing parameters related to diffusion and flow. The flow profile of pressure-driven flow inside a microcapillary is determined by using the fluorescence fluctuations of a small dye molecule. It was found that bacteria and microspheres are retarded in their flow by optical forces produced by the laser beam.**

The ability to screen particles is becoming more important in the fields of drug discovery and functional genomics. The groups of Eigen and Rigler have pioneered[1−4] high-throughput screening based on sensitive fluorescence detection methods, and an increasing number of applications are currently under development in the pharmaceutical industry.[5−10] Several groups reported detection of single molecules in microstructures using confocal detection schemes[11−18] or recently in submicrometer structures.[19] Here, a feasibility study is described to detect flowing, single fluorescent particles and fluorescent microorganisms in a microfluidic setup. This strategy fulfills a basic prerequisite for more complex applications such as screening of complex biolibraries with fluorescent ligands.[20−23]

Antibody libraries are the clearest example of biolibraries.[24] They are widely used today, to select for antibodies used in research and diagnosis and for applications in human medicine. These libraries comprise a large number (up to $>10^{10}$) different antibody fragments. Other examples of biolibraries are peptide libraries, cDNA libraries, and libraries used to select for protein variants suited for specific applications. Examples of the latter comprise protease inhibitors, proteases, $\beta$-lactamase, lipases, etc. Most biolibraries are displayed on bacteriophage, bacteria, and yeast cells and consist often of $>10^8$ genetically different variants. Selection usually involves several rounds wherein complexed ligands are captured batchwise followed by amplification in a bacterial host. After the last selection round, the remaining binders often have improved characteristics. An important drawback of display systems is the low specificity of the batchwise selection strategies, and the necessary amplification step may result in a loss of interesting binders as a consequence of genetic instability. To improve selection, it is necessary to enable specific detection. The advantages are paramount: fast and specific selection as well as a reduced loss of genetic diversity compared to the conventional methods. Required is a method to detect single complexes followed by selective extraction. This single-particle detection and

* Corresponding author: (e-mail) Ton.Visser@laser.bc.wau.nl.

[†] MicroSpectroscopy Centre, Laboratory of Biochemistry, Wageningen University.

[‡] Laboratory of Molecular Recognition and Antibody Technology, Wageningen University.

[§] Vrije Universiteit.

(1) Eigen, M.; Rigler, R. *Proc. Natl. Acad. Sci. U.S.A* **1994**, *91*, 5740−5747.
(2) Rigler, R. *J. Biotechnol.* **1995**, *41*, 177−186.
(3) Oehlenschläger, F.; Schwille, P.; Eigen, M. *Proc. Natl. Acad. Sci. U.S.A.* **1996**, *93*, 12811−12816.
(4) Dörre, K.; Brakmann, S.; Brinkmeier, M.; Han, K.-T.; Riebeseel, K.; Schwille, P.; Stephan, J.; Wetzel, T.; Lapczyna, M.; Stuke, M.; Bader, R.; Hinz, M.; Seliger, H.; Holm, J.; Eigen, M.; Rigler, R. *Bioimaging* **1997**, *5*, 139−152.
(5) Auer, M.; Moore, K. J.; MeyerAlmes, F. J.; Guenther, R.; Pope, A. J.; Stoeckli, K. A. *DDT* **1998**, *3*, 457−465.
(6) Wölke, J.; Ullmann, D. *DDT* **2001**, *6*, 637−645.
(7) Rudiger, M.; Haupts, U.; Moore, K. J.; Pope, A. J. *J Biomol. Screening* **2001**, *6*, 29−37.
(8) Hertzberg, R. P.; Pope, A. J. *Curr. Opin. Chem. Biol.* **2000**, *4*, 445−451.
(9) de Wildt, R. M.; Mundy, C. R.; Gorick, B. D.; Tomlinson, I. M. *Nat. Biotechnol.* **2000**, *18*, 989−994.
(10) Pope, A. J.; Haupts, U. M.; Moore, K. J. *DDT* **1999**, *4*, 350−362.
(11) Lee, Y. H.; Maus, R. G.; Smith, B. W.; Winefordner, J. D. *Anal. Chem.* **1994**, *66*, 4142−4149.
(12) Gösch, M.; Blom, H.; Holm, J.; Heino, T.; Rigler, R. *Anal. Chem.* **2000**, *72*, 3260−3265.
(13) Mathis, H. P.; Kalusche, G.; Wagner, B.; McCaskill, J. S. *Bioimaging* **1997**, *5*, 116−128.
(14) Dörre, K.; Stephan, J.; Lapczyna, M.; Stuke, M.; Dunkel, H.; Eigen, M. *J. Biotechnol.* **2001**, *86*, 225−236.
(15) Lyon, W. A.; Nie, S. *Anal. Chem.* **1997**, *1997*, 33400−3405.
(16) Zander, C.; Drexhage, K. H.; Han, K.-T.; Wolfrum, J.; Sauer, M. *Chem. Phys. Lett.* **1998**, *286*, 457−465.
(17) Lapos, J. A.; Manica, D. P.; Ewing, A. G. *Anal. Chem.* **2002**, *74*, 3348−3353.
(18) Nie, S.; Chiu, D. T.; Zare, R. N. *Anal. Chem.* **1995**, *67*, 2849−2857.
(19) Foquet, M.; Korlach, J.; Zipfel, W.; Webb, W. W.; Craighead, H. G. *Anal. Chem.* **2002**, *74*, 1415−1422.
(20) Schwalbach, G.; Sibler, A. P.; Choulier, L.; Deryckere, F.; Weiss, E. *Protein Expression Purif.* **2000**, *18*, 121−132.
(21) Georgiou, G. *Adv. Protein Chem.* **2001**, *55*, 293−315.
(22) Georgiou, G.; Stephens, D. L.; Stathopoulos, C.; Poetschke, H. L.; Mendenhall, J.; Earhart, C. F. *Protein Eng.* **1996**, *9*, 239−247.
(23) Stathopoulos, C.; Georgiou, G.; Earhart, C. F. *Appl. Microbiol. Biotechnol.* **1996**, *45*, 112−119.
(24) Ehrenberg, M.; Rigler, R. *Chem. Phys.* **1974**, *4*, 390−401.



10.1021/ac0256742 CCC: $22.00 
Published on Web 09/12/2002

sorting can be carried out using narrow channels in microfluidic biochips. However, before this methodology can be applied, it is necessary to understand the movement of macroscopic particles through the microchannels and to design detection and sorting strategies of fluorescent binders.

Therefore, we report on experiments with single fluorescent particles in a flowing liquid, with an emphasis on the possibilities of detecting these particles using confocal detection methods, in particular fluorescence correlation spectroscopy (FCS),[12,24−35] as well as following their movement through microcapillaries. These particles are used as a model for the detection of fluorescent ligand−receptor complexes, on bacteriophages, microspheres, bacteria, or yeast cells, which is based on fluorescence photon bursts upon passage through the confocal excitation volume.

Different fluorescent systems varying in size from small fluorescent molecules to intrinsically fluorescent *Escherichia coli* bacteria and macroscopic fluorescent microspheres were used in this study. In FCS, fluctuations in the fluorescence signal due to passage of single molecules through the confocal volume element (CVE) are detected. Because of the small volume involved (∼1 fL), background emission is largely reduced, and therefore, only photons emitted by single fluorophores excited in the CVE are detected. Due to the microscope optics, only a small fraction (∼3%) of emitted photons is detected. The fluctuations in fluorescence intensities are autocorrelated, yielding information about the number of fluorescent particles, diffusion properties, and chemical kinetics. Not only the autocorrelation traces but also the time window of the individual photons contain information about the fluorescent molecules such as number and brightness.[35−40] The obtained results contribute to the development of a system allowing specific and rapid detection and selection of binders from biolibraries.

## MATERIALS AND METHODS

**Theoretical Background.** Since flowing single fluorescent molecules are detected, the real-time autocorrelation of the fluorescence intensity fluctuations is used for the analysis of diffusion and flow. The diffusion rate can be determined by autocorrelating numerous photon events. The theoretical framework for applications of FCS in the analysis of uniform translation (plug flow) and laminar flow, superimposed on diffusion and active transport, was given by Magde et al.[28] Let us briefly summarize the expressions for the autocorrelation function describing diffusion only. Assuming a Gaussian detection volume, the autocorrelation function $G(\tau)$ can be written as[41]

$$G(\tau) = 1 + (1/N)A$$

where

$$A = \left(1 + \frac{\tau}{\tau_{\text{diff}}}\right)^{-1}\left[1 + \left(\frac{\omega_{xy}}{\omega_z}\right)^2\left(\frac{\tau}{\tau_{\text{diff}}}\right)\right]^{-1/2} \quad (1)$$

Here $N$ denotes the number of fluorescent particles, $\tau_{\text{diff}}$ is the diffusion time of the fluorescent particle (or its residence time in the CVE), and $\omega_{xy}$ *and* $\omega_z$ are the radius and length of the CVE, respectively, assuming that the spatial intensity distribution of the laser beam has a Gaussian 3D profile. The structure parameter, $\omega_z/\omega_{xy}$, is of importance since it reflects the optical quality of the CVE. It usually amounts to 5−10 for aqueous samples in chambers separated by a flat borosilicate bottom. The translational diffusion constant $D_{\text{trans}}$ is related to the diffusion time $\tau_{\text{diff}}$:

$$D_{\text{trans}} = {\omega_{xy}}^2/4\tau_{\text{diff}} \quad (2)$$

The recorded autocorrelation curves are analyzed using in-house-developed global analysis software. To determine the structure parameter, the dye Rhodamine Green was used for calibration because of its well-determined[27,42] $D_{\text{trans}}$ of $2.8 \times 10^{-10}$ $m^2 \cdot s^{-1}$. $\tau_{\text{diff}}$ and $\omega_z/\omega_{xy}$ were obtained by fitting the autocorrelation data curves to eq 1, whereas the square of the beam waist, ${\omega_{xy}}^2$, was obtained from eq 2. The volume of the confocal volume element ($V_{\text{CVE}}$) can be estimated from

$$V_{\text{CVE}} = \pi {\omega_{xy}}^2 \omega_z \quad (3)$$

When there is active transport in the form of laminar flow, the autocorrelation function $G(\tau)$ changes to[12,43,44]

$$G(\tau) = 1 + (1/N)A e^{-[(\tau/\tau_{\text{flow}})^2 A]} \quad (4)$$

where $\tau_{\text{flow}}$ is the average flow time of the fluorescent particles through the detection volume. In the following we refer to eq 4 as the fcs-flow model. The flow velocity $v$ is given by

$$v = \omega_{xy}/\tau_{\text{flow}} \quad (5)$$

The minimum flow velocity that can be measured is determined by Brownian diffusion. When the flow velocity is too small,


(25) Ehrenberg, M.; Rigler, R. *Q. Rev. Biophys.* **1976**, *9*, 69−81.
(26) Elson, E. L.; Magde, D. *Biopolymers* **1974**, *13*, 1−27.
(27) Magde, D.; Elson, E. L.; Webb, W. W. *Biopolymers* **1974**, *13*, 29−61.
(28) Magde, D.; Webb, W. W.; Elson, E. L. *Biopolymers* **1977**, *17*, 377−412.
(29) Aragón, S. R.; Pecora, R. *Biopolymers* **1975**, *14*, 119−138.
(30) Aragón, S. R.; Pecora, R. *J. Chem. Phys.* **1976**, *64*, 1791−1803.
(31) Winkler, T.; Kettling, U.; Koltermann, A.; Eigen, M. *Proc. Natl. Acad. Sci. U.S.A.* **1999**, *96*, 1375−1378.
(32) Koltermann, A.; Kettling, U.; Bieschke, J.; Winkler, T.; Eigen, M. *Proc. Natl. Acad. Sci. U.S.A.* **1998**, *95*, 1421−1426.
(33) Thompson, N. L. In *Topics in Fluorescence Spectroscopy*.; Lakowicz, J. R., Ed.; Plenum Press: New York, 1991; Vol. 1, pp 337−378.
(34) Rigler, R.; Mets, U.; Widengren, J.; Kask, P. *Eur. Biophys. J.* **1993**, *22*, 169−175.
(35) Widengren, J.; Mets, Ü.; Rigler, R. *J. Phys. Chem.* **1995**, *99*, 13368−13379.
(36) Chen, Y.; Muller, J. D.; So, P. T.; Gratton, E. *Biophys. J.* **1999**, *77*, 553−567.
(37) Kask, P.; Palo, K.; Ullmann, D.; Gall, K. *Proc. Natl. Acad. Sci. U.S.A.* **1999**, *96*, 13756−13761.
(38) Kask, P.; Palo, K.; Fay, N.; Brand, L.; Mets, U.; Ullmann, D.; Jungmann, J.; Pschorr, J.; Gall, K. *Biophys. J.* **2000**, *78*, 1703−1713.
(39) Kask, P.; Gunther, R.; Axhausen, P. *Eur. Biophys. J.* **1997**, *25*, 163−169.
(40) Enderlein, J.; Kollner, M. *Bioimaging* **1998**, *6*, 3−13.
(41) Widengren, J.; Rigler, R. *Cell. Mol. Biol.* **1998**, *44*, 857−879.
(42) Rigler, R.; Widengren, J.; Mets, U. In *Fluorescence spectroscopy. New methods and applications*; Wolfbeis, O. S., Ed.; Springer-Verlag: Berlin, 1991; pp 13−24.
(43) Brinkmeier, M.; Dörre, K.; Stephan, J.; Eigen, M. *Anal. Chem.* **1999**, *71*, 609−616.
(44) Brinkmeier, M.; Rigler, R. *Exp. Tech. Phys.* **1995**, *41*, 205−210.

it becomes difficult to distinguish between diffusion alone and diffusion superimposed on flow. Therefore, $\tau_{flow}$ must be distinctly shorter than the diffusion time, $\tau_{diff}$, to recover the flow velocity from the analysis.

**Setup.** The experimental apparatus is built around a ConfoCor I (Carl Zeiss, Jena, Germany), an inverted confocal fluorescence microscope, especially designed to perform fluorescence correlation spectroscopy.[45] We used the 488- or 514-nm laser lines from an argon laser to excite, respectively, enhanced green fluorescent protein (EGFP)[46] in *E. coli*, microspheres, and enhanced yellow fluorescent protein (EYFP)[46] in *E. coli*. A Zeiss 40 × 1.2 NA water immersion objective focuses the laser beam into a diffraction-limited spot. Neutral density filters were used to decrease the incident laser power.[47] Usually a 96-well plate with borosilicate bottom (Whatman, Clifton, NJ) is used to contain the samples. In this work a 100 × 100 $\mu$m$^2$ silica microcapillary (Polymicro Technologies Inc, Phoenix, AZ) is used and mounted so that the laser spot (CVE) is located exactly in the middle of the capillary. Fluorescence photons emitted in the laser spot are detected by an avalanche photodiode (APD) (EG&G, Quebec, Canada) and autocorrelated in real time using an AVL-5000 autocorrelator card (ALV, Langen, Germany) in a Windows computer. We used the ConfoCor I software to control this card and to store the processed data. A digital storage scope (Agilent Technologies, Palo Alto, CA) was used to observe the photon stream. With this instrument we observed that photons are converted by the APD to TTL pulses lasting 50 ns.

The capillary is connected via Valco connectors (Valco Instruments, Houston, TX) to an injection system (valve V7, Pharmacia, Uppsala, Sweden) and a standard FPLC pump (P-500, Pharmacia LKB, Uppsala, Sweden). With this system, samples (typically 0.025−2 mL, depending on the sample loop) can be injected in the flow of buffer (flow rate typically less than 5 mL·h$^{-1}$). A 1:3 flow splitter was used to obtain lower flow rates than the pump could deliver. The applied flow rate was measured through weighing of the pumped volume. The capillary fiber is coated with polyimide, which is of importance for the mechanical stability of the glass capillary. Prior to positioning the capillary on top of the objective, the coating was burnt off with a moderate flame (∼1 cm). Cleaning of the fiber with soft tissue resulted in a surface of good optical quality.

**Reagents Used.** Rhodamine Green, Rhodamine 6Gm and Green-yellow fluorescent microspheres were obtained from Molecular Probes (Leiden, The Netherlands).

**Fluorescent Bacteria Preparation.** The open reading frame of EYFP cDNA was amplified by the polymerase chain reaction (PCR) from EYFP full-length cDNA and was cloned into a pTYB11 vector (New England Biolabs, Impact vector system) using the following primers: YFPfor (5′ GGTGGTTGCTCTTCCAACATG-GTGAGCAAGGGCG 3′) and YFPrev (5′ GGTGGTGGATTCT-TACTTGTACAGCTCG 3′). The pTYB11-EYFP construct was introduced into the BL21 DE3 *E. coli* bacteria strain for high expression levels. The cells were induced by adding 0.3 mM IPTG and grown at 20 °C. The cells were harvested after 3 h of induction and washed with buffer (50 mM Tris pH 8, 120 mM KCl, and 15% glycerol). Similar procedures using an open reading frame of EGFP full-length cDNA yielded *E. coli* harboring EGFP. The *E. coli*-EYFP (and *E. coli*-EGFP) cells were stored at −80 °C. EYFP and EGFP were obtained as described recently[48,49]

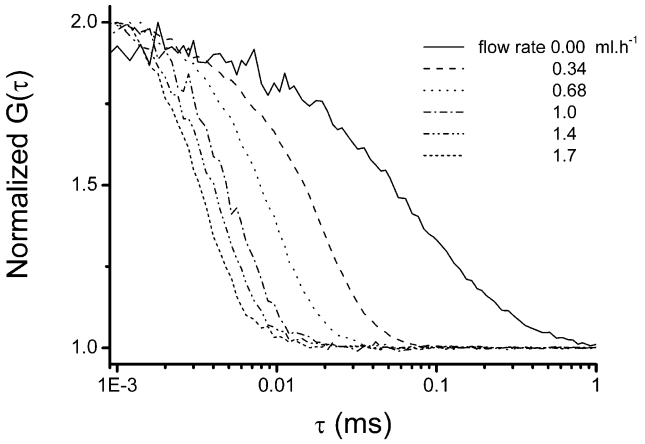


Figure 1. Normalized autocorrelation traces of 5 nM Rhodamine Green in water at different flow rates.

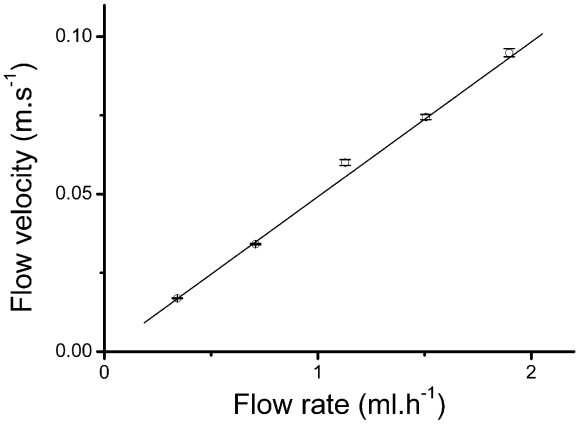


Figure 2. Linearity of flow velocities recovered from analysis with the fcs-flow model vs the applied flow rate through the capillary.

## RESULTS AND DISCUSSION

**Calibration.** Calibration of the optical system was performed using 5 nM Rhodamine Green introduced in the capillary. The parameters obtained were used to calculate the radius and height of the detected confocal volume element and the structure parameter (see eqs 2 and 3). The confocal laser spot (488 nm) was focused in the middle of the capillary. First, the position of the 40-$\mu$m pinhole in the instrument was optimized using an automated procedure. Next, five autocorrelation curves collected during 1 min/curve were obtained. Using these curves, the structure parameter of this setup was determined using eqs 1 and 2. Typically, Rhodamine Green gave a diffusion time of 90 $\mu$s and a structure parameter of 15 resulting in a CVE of ∼1.5 fL (beam waist $\omega_{xy}$ ∼320 nm). The square capillary gave structure parameters that are about twice as large as usually found by using multiwell plates. This discrepancy was attributed to the less perfect

(45) Hink, M. A.; van Hoek, A.; Visser, A. J. W. G. *Langmuir* **1999**, *15*, 992−997.
(46) Tsien, R. Y. *Annu. Rev. Biochem.* **1998**, *67*, 509−544.
(47) Visser, A. J. W. G.; Hink, M. A. *J. Fluoresc.* **1999**, *9*, 81−87.
(48) Visser, N. V.; Hink, M. A.; Borst, J. W.; van der Krogt, G. N. M.; Visser, A. J. W. G. *FEBS Lett.* **2002**, *521*, 31−35.
(49) Griep, R. A.; van Twisk, C.; van der Wolf, J. M.; Schots, A. *J. Immunol. Methods* **1999**, *230* (1−2), 121−130.

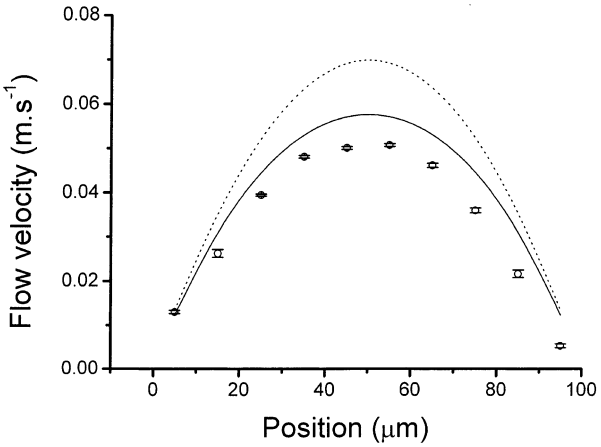


Figure 3. Flow velocity (experimental points) of Rhodamine Green through the width of the capillary showing a parabolic curve with the highest flow in the middle. Theoretical flow profiles for laminar flow in cylindrical (dotted line) and square (solid line) tubes are also presented.

optical quality of the capillary fiber. Multiwell plates contain borosilicate glass sheets, which have a much better flatness.

The autocorrelation curve was measured using different pump speeds (see Figure 1). The diffusion time was fixed in the fcs-flow model (eq 4) to determine the flow velocities (eq 5) in the capillary from flow experiments with Rhodamine Green. We then fitted the experimental autocorrelation traces to the fcs-flow model and obtained, a linear correlation between the pump settings and the recovered flow velocity (see Figure 2).

**Flow Profile in Capillary.** For flow profiling in the capillary, we followed the procedure outlined by Gösch et al.[12] Rhodamine Green (2.5 nM) was used as indicator dye, and the lowest possible pump speed setting of 1 mL·h$^{-1}$ (without splitter) was applied. The diffraction-limited laser spot (beam waste ($\omega_{xy}$) 320 nm) was first focused in the middle of the capillary and spatially scanned through the width of the capillary with steps of 10 $\mu$m. The flow velocity was obtained by global fitting of several 1-min-long autocorrelation curves to the fcs-flow model. The recovered flow velocity of the liquid in the middle of the 100 × 100 $\mu$m$^2$ capillary was ~5 × 10$^{-2}$ m·s$^{-1}$ when the pump speed was set to its lowest value of 1 mL·h$^{-1}$. Using the recovered flow velocity, the apparent residence time of a single, flowing Rhodamine Green molecule in the CVE (assuming a diameter of twice the beam waste) is then ~13 $\mu$s. The recovered flow velocity is comparable to the average flow velocity that can be calculated from the pump speed and the geometry of the capillary fiber. The average flow velocity through the capillary is ~3 × 10$^{-2}$ m·s$^{-1}$. The difference between both values can be attributed to the parabolic flow rate profile as shown in Figure 3: the highest flow velocity is in the middle of the capillary. Near the wall, the flow is very slow. This parabolic flow profile is typical for laminar pressure-driven flow in tubes and was already observed by Poiseuille in the 18th century.[50] Similar results were reported by Gösch et al.[12]

The flow profile for a cylindrical tube is given by Poiseuille's law:[51]

$$v_x = (1/4\mu)(R^2 - x^2)\chi \quad (6)$$

where $v_x$ is flow velocity at position $x$ along the axis, $R$ is radius of the tube, and $\mu$ is the dynamic viscosity of the liquid. The pressure drop per length of a cylindrical tube is given by[51]

$$\chi = -\Phi 8\mu/\pi R^4 \quad (7)$$

where $\Phi$ is the flow rate. Using eqs 6 and 7, the measured flow profile deviates from this theoretical curve using $\Phi = 2.78 \times 10^{-10}$ m$^3$·s$^{-1}$ (flow rate of 1 mL·h$^{-1}$), $\mu = 1.002 \times 10^{-3}$ kg.m$^{-1}$·s$^{-1}$, and $R$= 50 $\mu$m (see Figure 3).

Let us now discuss the velocity distribution in a rectangular tube for which an expression has been derived by Pozrikidis:[52]

The velocity distribution for a rectangular tube can be expressed by an infinite series:[52]

$$v_x(y,z) = \frac{\chi + \rho g_x}{2\mu} b^2 \left[ 1 - \frac{z^2}{b^2} + 4\sum_{n=1}^{\infty} \frac{(-1)^n}{\alpha_n{}^3} \frac{\cosh(\alpha_n(y/b))}{\cosh(\alpha_n(a/b))} \cos\left(\alpha_n \frac{z}{b}\right) \right] \quad (8)$$

where $v_x(y,z)$ is the velocity at point $x$ at area ($y$,$z$), 2$a$ and 2$b$ are the side lengths of the rectangular tube, $\rho g_x$ is the product of density and gravity, and $\alpha_n = \pi(n - (1/2))$. For the flow rate $\Phi$, the following equation has been obtained:[52]

$$\Phi = \frac{\chi + \rho g_x}{3\mu} 4ab^3 \left[ 1 - 6\frac{b}{a}\sum_{n=1}^{\infty} \frac{1}{\alpha_n{}^5} \tanh\left(\alpha_n \frac{a}{b}\right) \right] \quad (9)$$

Figure 3 shows the theoretical flow profile in our square capillary using $\Phi = 2.78 \times 10^{-10}$ m$^3$·s$^{-1}$, $\rho g_x = 0$, $a = b = 50 \times 10^{-6}$ m, $\mu = 1.002 \times 10^{-3}$ kg·m$^{-1}$·s$^{-1}$, and $z = 0$. Now, the theoretical curve gives a better approximation to the experimental data than the cylindrical model.

**Bacteria in a Capillary.** *E. coli* cells harboring the fluorescent protein EYFP or EGFP were injected into the capillary. Brownian movement of the bacteria causes them to pass through the detection volume, creating photon bursts of >10$^6$ photons/s (see Figure 4A). The photon stream was autocorrelated in real time (see Figure 4B). The bacteria had a $\tau_{diff}$ in the order of several milliseconds. When the bacteria flowed through the capillary, the autocorrelation curves apparently show a much shorter diffusion time (see Figure 5). The photon bursts dropped dramatically to 10−75 × 10$^3$ photons/s because the residence time of the fluorescent particles in the detection volume is much shorter. Upon increasing the concentration of the bacterial cell suspension, the time between single events decreased and the amplitude of the autocorrelation trace became smaller (see Figure 6). The

(50) Sutera, S. P. *Annu. Rev. Fluid Mech.* **1993**, *25*, 1−19.

(51) Resnick, R.; Halliday, D.; Krane, K. S. *Physics*, 4 ed.; John Wiley & Sons: Inc.: Toronto, Canada, 1992.

(52) Pozrikidis, C. *Fluid dynamics: theory, computation, and numerical simulation*; Kluwer Academic Publishers Group: Dordrecht, The Netherlands, 2001.

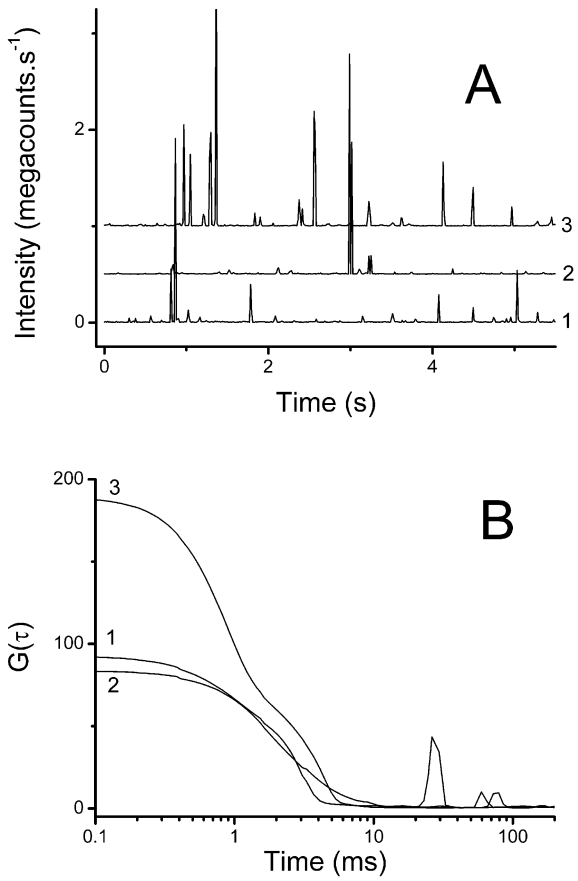


Figure 4. (A) Photon bursts observed when *E. coli* bacteria containing EYFP diffuse through the femtoliter detection volume. Three curves have been stacked for reasons of clarity. (B) The autocorrelation curves show a large spread in diffusion times. The three measurements were 5.5 s long.

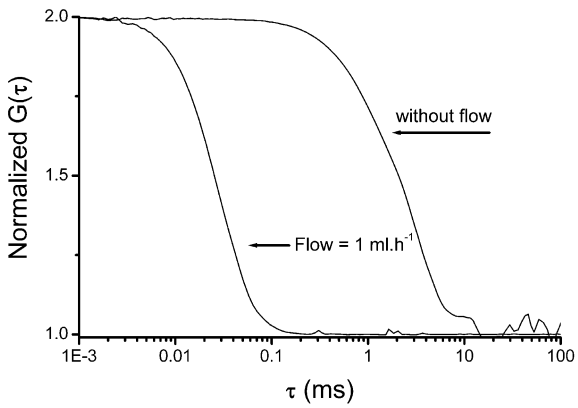


Figure 5. Normalized autocorrelation traces of *E. coli* bacteria containing EYFP with and without flow measured during a 1-min period.

amplitude of the autocorrelation curves, $G(0)$, scales inversely with the number of particles (see eq 1).

In the absence of flow, we observed that the diffusion time of a single bacterium was between 1 and 15 ms. Diffusion times depend on the followed trajectory through the confocal volume element. The volume of the CVE is similar to that of bacteria. This has implications for the applied fcs-flow model, since this model is based upon traveling of relatively small fluorescent molecules through the much larger CVE.[26] It can be imagined that the exact value of $\tau_{diff}$ is dependent on that part of the particle, which is transiently in the CVE. The $\tau_{diff}$ will be shorter than expected when only the tips of a bacterial cell are in the CVE. Therefore, the value of $\tau_{diff}$ is not accurately defined. For more accurate determination of $\tau_{diff}$, the CVE must be made larger.

The flow velocity itself was calculated from $\tau_{flow}$ using eq 5. The flow velocity of bacteria is smaller than the flow velocity of relatively small molecules such as EYFP protein (27 kDa) or Rhodamine Green (see Figure 7, in which the flow velocities obtained using the fcs-flow model versus the laser power have been summarized for all fluorescent systems studied). The pump flow was held constant at a flow rate of 1 mL·h$^{-1}$. Furthermore, the apparent flow velocity of bacteria depends on the laser intensity. Experiments in which mixtures of fluorescent and nonfluorescent bacteria were used showed that there is no influence of the nonfluorescent bacteria on the apparent flow velocity. Because they have a better-defined shape, the flow velocity of fluorescent microspheres of different sizes was measured to investigate the nature of the dependence on laser intensity.

**Microspheres in a Capillary.** Green-yellow fluorescent microspheres of sizes ranging from 0.11 to 2.2 $\mu$m were introduced in the capillary flow, and the flow velocity was determined as described in the previous paragraph. Initially, we used a fixed value (the average of many measurements) for $\tau_{diff}$ in the analysis of flow experiments at fixed flow rates. This procedure was described for small molecules, but experiments were not carried out for macroscopic particles.[12] When $\tau_{diff}$ is not fixed in the fitting procedure, the fit improved considerably signified by a lower, relative $\chi^2$ (goodness-of-fit criterion). However, no significant influence was found on the $\tau_{flow}$ values. This is illustrated in Table 1, summarizing the recovered parameter values of experiments of 0.56-$\mu$m microspheres with different laser light intensities. It is also clear from the data in Table 1 that $\tau_{flow}$ and $\tau_{diff}$ become longer when the laser intensity increases and that there is a distinct correlation between their values. The physical meaning of the apparently anomalous $\tau_{flow}$ and $\tau_{diff}$ will be addressed in the next paragraph. The laser intensity has the same effect as observed in the experiments with fluorescent bacteria: The higher the laser intensity, the slower the microspheres appeared to flow (Figure 7). Furthermore, larger microspheres are flowing slower than smaller ones. The relatively small EYFP protein and the calibration dye Rhodamine Green have the same flow velocity that is independent of the applied laser intensity. The rod-shaped *E. coli* bacteria flow with an apparent velocity similar to that of spheres of 0.22 $\mu$m.

Similarly, as shown for Rhodamine Green (Figure 2) the apparent flow velocities of microspheres of 0.22- and 0.56-$\mu$m size scale linearly with the pump settings (results not shown).

Further evidence for retardation of particles during detection came from direct observations of the photon pulses of flowing fluorescent microspheres using a digital storage oscilloscope (flow rate: 1 mL·h$^{-1}$, 2 × 10$^6$ 0.56-$\mu$m microspheres·mL$^{-1}$, 125-$\mu$W 488-nm laser power). An individual photon burst typically consists of 100−150 photon pulses (counts), and a single burst lasts on average approximately 50−60 $\mu$s. This number is comparable to the results from fcs-flow analysis of flowing microspheres (see $\tau_{flow}$ in Table 1). These photon bursts therefore represent the passage of one fluorescent particle. The duration of the burst is

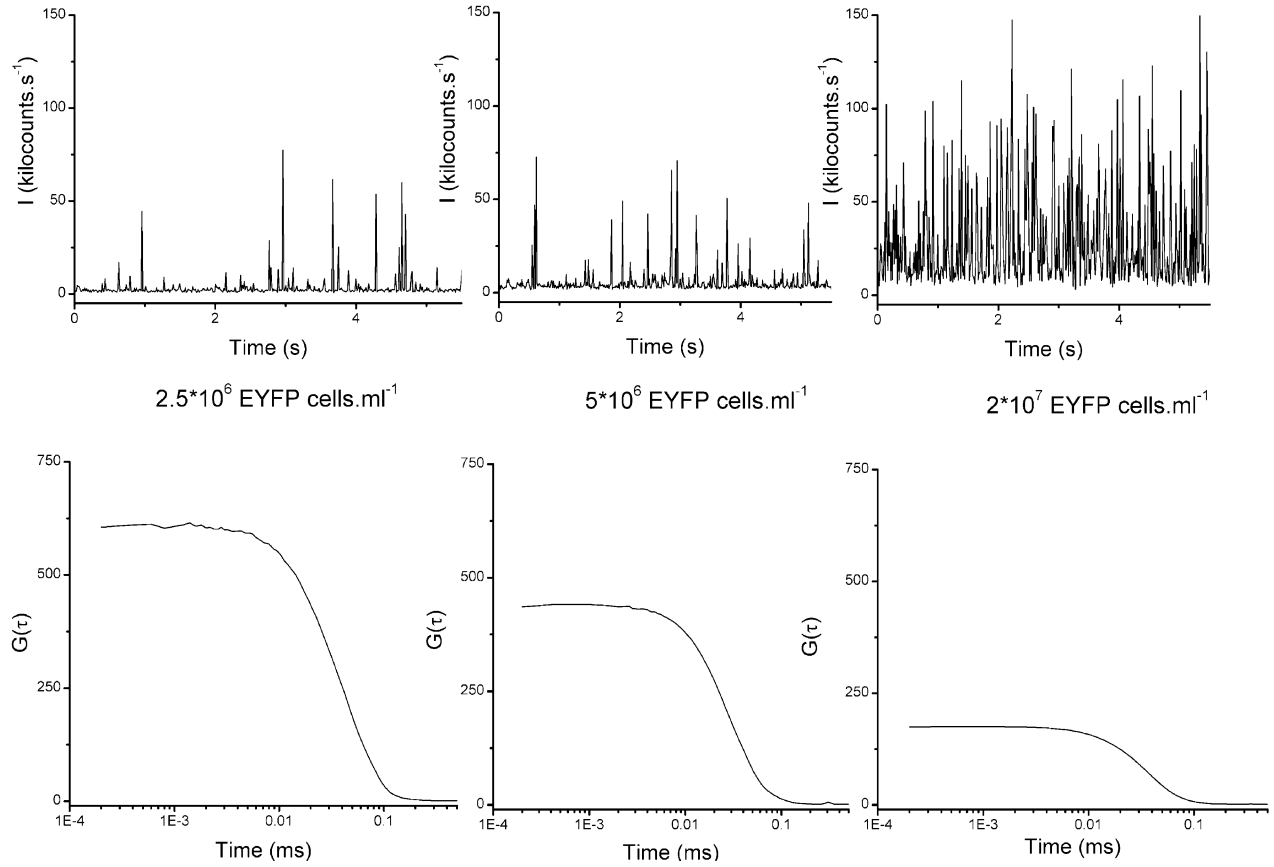


Figure 6. Influence of the concentration of *E. coli* bacteria containing EYFP on the fluorescence intensity traces (upper panel) and the corresponding autocorrelation curves (lower panel) at a flow rate of 1 mL·h$^{-1}$. The autocorrelation curves were obtained during a 1-min period.

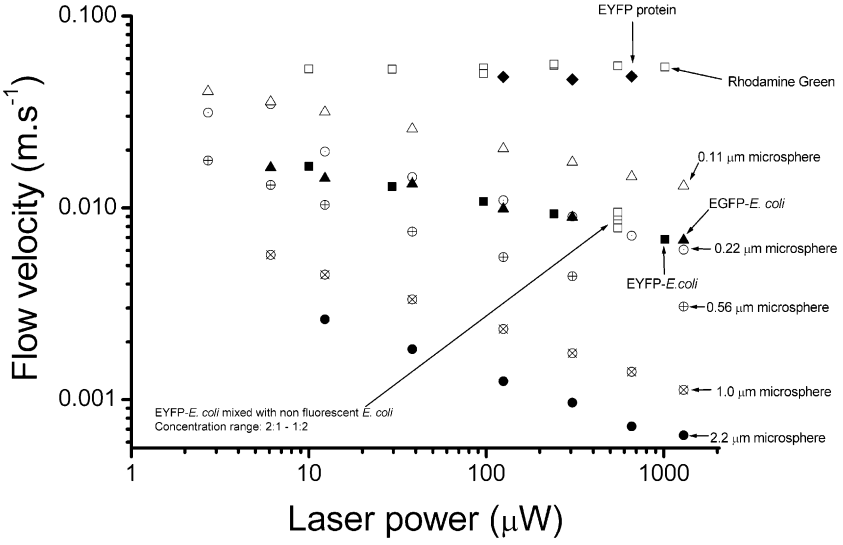


Figure 7. Variation of laser power vs flow velocity of small molecules such as isolated EYFP and Rhodamine Green. In contrast, the laser intensity influences the (apparent) flow velocity of macroscopic particles such as bacteria and microspheres. Larger particles are more retarded than smaller particles, and higher laser power leads to more retardation.

almost 5 times larger than the 13-$\mu$s residence time of a flowing Rhodamine Green molecule. In other words, microspheres are retarded in their flow during passage through the CVE.

With the FCS instrument, the photons are counted and stored in so-called bins. The minimum bin time was determined by the electronics and was 13.5 ms. In the 13.5-ms bins, we observed, for example, bursts as high as $10^6$ photons/s, when fluorescent bacteria passively diffused through the CVE. When they flowed through the capillary with a velocity of $5 \times 10^{-2}$ m·s$^{-1}$, photon bursts of $5 \times 10^4$ photons/s were observed corresponding to ~675 photons counted per bin. These numbers are based on the average of many particles and are not representative of the photon burst emitted by a single, passing particle. However, we can estimate the number of passing particles per unit time through the CVE. The top right panel of Figure 6 shows the measured photon intensity of passing fluorescent bacteria through the CVE. The

Table 1. Influence of $\tau_{diff}$ Fixation on the $\tau_{flow}$ of Microspheres Using the fcs-Flow Model[a]

| | A | | | | | B | | |
|---|---|---|---|---|---|---|---|---|
| laser power, $\mu$W | $\tau_{flow}$, $\mu$s | confidence interval (67%) | $\tau_{diff}$, $\mu$s | confidence interval (67%) | $\chi$2 | $\tau_{flow}$, $\mu$s | confidence interval (67%) | $\chi$2 |
| 1295 | 102 | 99.8−103 | 130 | 123−136 | $9.0 \times 10^{-5}$ | 95.1 | 91.5−98.2 | $2.4 \times 10^{-3}$ |
| 306 | 70.9 | 70.8−71.4 | 85.9 | 83.4−87.8 | $1.4 \times 10^{-4}$ | 68.6 | 64.6−72.2 | $9.3 \times 10^{-3}$ |
| 125 | 56.4 | 56.4−56.8 | 68.2 | 56.8−70.1 | $4.3 \times 10^{-4}$ | 56.2 | 52.9−59.4 | $2.4 \times 10^{-2}$ |
| 38.2 | 41.5 | 41.5−41.8 | 52.0 | 50.0−54.0 | $2.0 \times 10^{-3}$ | 42.3 | 40.0−44.5 | $6.2 \times 10^{-2}$ |
| 12.3 | 30.2 | 30.1−30.3 | 42.4 | 40.3−44.4 | $7.5 \times 10^{-3}$ | 31.6 | 30.3−33.1 | 0.13 |
| 6.1 | 23.7 | 23.7−23.9 | 38.1 | 36.2−40.5 | $1.8 \times 10^{-2}$ | 25.3 | 24.1−26.4 | 0.21 |
| 2.7 | 17.9 | 17.4−17.9 | 32.4 | 29.9−35.1 | $6.1 \times 10^{-2}$ | 19.0 | 18.4−19.7 | 0.39 |

[a] Flowing microspheres (0.56 $\mu$m, 1 mL·h$^{-1}$) are investigated using different laser intensities. The autocorrelation curves are fitted to the fcs-flow model with a fixed (B) and nonfixed (A) $\tau_{diff}$ parameter. Microspheres have a diffusion constant in the range of several milliseconds. Fixation of $\tau_{diff}$ to 2.5 ms has no profound effect on the obtained $\tau_{flow}$ values, but on the goodness of fit signified by a higher relative $\chi^2$. Confidence intervals were obtained after an exhaustive search as described by ref 58.

averaged photon intensity was calculated to be 27 000 photons/s (corrected for background). When we assume that one particle emits 100 photons, then on average 3.6 particles are counted in one bin. This corresponds to ~270 particles/s.

**Optical Forces on Microspheres.** The obtained flow velocity using large fluorescent particles such as bacteria and microspheres is smaller than the flow velocity of calibration dyes. To investigate this further, the behavior of microspheres was observed using different laser light intensities. Several 2.2-$\mu$m microspheres in a 96-well plate with a flat borosilicate bottom could be viewed through the ocular eyepiece of the ConfoCor I setup. The microspheres could be trapped with a laser power of ~1 mW using a wavelength of 488 nm. A captured microsphere was seen as a fluorescent particle around the focal point of the laser beam, and it did not move when the well plate was slowly moved using the translation stage of the microscope (nontrapped particles did move). The trap could easily lose the particle by a fast movement of the well plate. It was not possible to visibly trap smaller particles or use less laser power. In other words, the influence due to radiation pressure on dielectric particles of micrometer size such as microspheres is weak but present and plays a role in the retardation of flowing particles. The flow retardation is related to optical laser trapping[53−57] since that phenomenon depends on the laser intensity and particle size. Now the correlation between $\tau_{flow}$ and $\tau_{diff}$ as a function of the laser intensity becomes clear (see Table 1). When the flow is retarded, the diffusion must be equally affected, since free diffusion does not take place any more.

Let us now try to estimate the forces that act on these particles. Optical forces are usually defined by the following relationship:[54,56,57]

$$F_{trap} = Q\eta P/c \tag{10}$$

where $Q$ is a dimensionless efficiency parameter, $\eta$ is the refractive index of the surrounding medium, $c$ is the speed of light in vacuo, and $P$ is the incident laser power. The efficiency parameter $Q$ represents the fraction of the power used to exert force. It takes into account the convergence angle, spot size, wavelength, polarization, and point spread function of the incident light. $Q$ also contains parameters related to the optical properties of the trapped particle such as size, shape, and refractive index. The maximum force that can be created is when $Q = 1$. When the laser power is 1 mW, the maximum force is equal to ~4.4 pN.

The drag force is given by Stokes law:[56]

$$\Delta F_{drag} = -6\pi\mu\Delta v r \tag{11}$$

where $\mu$ is the dynamic viscosity, $r$ the radius of the sphere, and $\Delta v$ the difference between initial flow velocity and measured flow velocity during passage through the CVE. When we use the Stokes equation to obtain the drag force for 0.56-$\mu$m spheres using $\Delta v$ ($\Delta v \approx 0.047$ m·s$^{-1}$; see Figure 7), drag forces are between 300 and 400 pN. These numbers are clearly too high. We can draw two conclusions from these results. Optical trapping theory for particles in a flow has to be critically examined. For cases where the particles are of a size similar to the CVE, FCS experiments have to be repeated for an optical geometry in which the CVE is much larger than the particle size.

## CONCLUSIONS

We have used FCS to detect flowing fluorescent particles and molecules in a capillary. With these experiments, the basic prerequisites for confocal detection of fluorescent particles in complex microfluidic biochips have been fulfilled. In these biochips, detection and sorting of biolibraries takes place within milliseconds. The parameters for successful detection have been elucidated. For example, the temporal detection window of a flowing fluorescent particle depends on the bulk flow rate and can be as low as 50−100 $\mu$s. In this time window, a photon burst of ~100 photons can successfully be distinguished from the ubiquitous background.

The flow velocity can be determined from a fcs-flow model. For large particles (>0.2 $\mu$m), the recovered flow velocities are dependent on the laser intensity and their radius. These particles seem to be retarded in the confocal detection volume due to optical

(53) Ashkin, A. *Phys. Rev. Lett.* **1970**, *24*, 156−159.
(54) Ashkin, A. *Biophys. J.* **1992**, *61*, 569−582.
(55) Ashkin, A. *Proc. Natl. Acad. Sci. U.S.A.* **1997**, *94*, 4853−4860.
(56) Wright, W. H.; Sonek, G. J.; Berns, M. W. *Appl. Opt.* **1994**, *33*, 1735−1748.
(57) Svoboda, K.; Block, S. M. *Annu. Rev. Biophys. Biomol. Struct.* **1994**, *23*, 247−285.
(58) Beechem, J. M.; Gratton, E.; Ameloot, M.; Knutson, J. R.; Brand, L. In *Topics in Fluoresence Spectroscopy*; Lakowicz, J. R., Ed.; Plenum Press: New York, 1991; Vol. 2.

forces. The real nature of this retardation by laser illumination requires further investigation.

When using a microfluidic biochip setup for screening of particle-based biolibraries, one should take into account that the time needed to detect particles with highly focused laser light cannot be easily determined from the flow velocity of the liquid. This time should be found empirically.

## ACKNOWLEDGMENT

This research has been supported by the Technology Foundation STW, the applied science division of The Netherlands Organization for Scientific Research NWO and the technology program of the Ministry of Economic Affairs (Grant WBI 4797). We thank Jan Willem Borst for making available fluorescent proteins and fluorescent bacteria. We appreciate stimulating discussions with Marileen Dogterom, Mark Hink, Robin M. Schoemaker, and Jan Rinze Peterzon.

Received for review April 2, 2002. Accepted August 5, 2002.

AC0256742